Available online at www.sciencedirect.com

jmr&t Journal of Materials Research and Technology

journal homepage: www.elsevier.com/locate/jmrt

Original Article

Effect of crack width on electromagnetic interference shielding effectiveness of high-performance cementitious composites containing steel and carbon fibers

Soonho Kim, Yun Sik Jang, Taekgeun Oh, Seung Kyun Lee, Doo-Yeol Yoo *

Department of Architectural Engineering, Hanyang University, 222 Wangsimni-ro, Seongdong-gu, Seoul, 04763, Republic of Korea

ARTICLE INFO

Article history:
Received 4 March 2022
Accepted 6 July 2022
Available online 14 July 2022

Keywords:
High-performance fiber-reinforced cementitious composites
Carbon fiber
Electromagnetic interference shielding
Mechanical properties
Crack width

ABSTRACT

In this study, the effects of carbon fibers and crack widths on the electromagnetic interference (EMI) shielding effectiveness of high-performance fiber-reinforced cementitious composites (HPFRCCs) with 2 vol.% straight steel fibers were evaluated. To this end, 0.2 vol.% carbon fibers were added and four penetrated pre-crack widths ranging from 0.02 to 0.2 mm were applied under tension. The tensile strength and electrical resistance of the composites were also investigated. The test results indicated that adding 0.2% carbon fibers effectively enhanced the tensile strength, electrical conductivity, and shielding effectiveness of the HPFRCC. Furthermore, the electrical conductivity was improved by 224%, and a 27% higher shielding effectiveness was achieved. A shielding effectiveness of 48.5 dB at 1 GHz was achieved with a specimen thickness of 25 mm. Tiny cracks with a width of 20 μm significantly reduced the EMI shielding effectiveness of the HPFRCC by approximately 40%. For the plain HPFRCC, the shielding effectiveness was not significantly affected by the crack width, as it was thoroughly cracked. The benefits of adding carbon fibers for improving the shielding effectiveness disappeared at crack widths greater than 0.1 mm. Thus, the addition of carbon fibers was effective only for HPFRCCs without cracks or with very tiny cracks of less than 40 μm.

1. Introduction

Carbon-based materials such as carbon nanotubes (CNTs), carbon fibers, and graphene have received attention from civil and architectural engineers as new ingredients of concrete because of their benefits of enhancing the mechanical properties [1–3] and durability [4,5] of concrete. In addition, these materials can improve electrical conductivity, which enables the material to have additional functions, such as self-sensing [6–8] and electromagnetic interference (EMI) shielding [9–11]. Four-probe resistivity measurements performed by Yoo et al.

* Corresponding author.
E-mail address: dyyoo@hanyang.ac.kr (D.-Y. Yoo).
https://doi.org/10.1016/j.jmrt.2022.07.041

[6] demonstrated that carbon fibers were more effective for improving the electrical conductivity of cement paste at low volume fractions than CNTs, graphene, graphite nanofibers, and graphene oxide, whereas CNTs were most effective for increasing the conductivity at high volume fractions. Chung [12] noted that steel micro-fibers with a diameter of 8 μm were most effective for lowering the electrical resistivity of cement composites, and carbon fibers with a diameter of 15 μm were more effective for decreasing the resistivity than carbon nanofibers, coke powder, or graphite nanofibers. Because shielding effectiveness is a function of electrical conductivity [13], carbon-based materials, which are more effective for lowering the electrical resistivity, can improve EMI shielding effectiveness. In addition to the carbon-based materials, highly conductive and thin EMI shielding materials such as liquid-metal based films, water-based conductive ink, and conductive fabric have been developed in recent years, providing EMI shielding effectiveness of 78.2 dB at 20 μm thickness [14–17].

The use of electronic devices has grown rapidly, leading to an increase in electromagnetic pollution beyond environmental pollution [18]. According to the World Health Organization (WHO) [19], short-term exposure to very high levels of electromagnetic fields is harmful to health, and severe EMI pollution results in considerable harm to the human body and interrupts normal operation of body organs [20]. To shield electromagnetic waves, researchers [21–24] have attempted to develop EMI-resistant cementitious composites because they are cost-effective and can be used as structural elements in buildings. Fan et al. [21] studied the influence of stainless steel dust as an additional admixture to cement composites and determined that it increased the EMI shielding effectiveness. An incident electromagnetic wave was decreased by approximately 60%, and a stainless steel dust mixture with a thickness of 5 mm provided shielding of 6–9 dB. Khushnood et al. [23] noted a significant enhancement in the EMI shielding effectiveness of cement composites with the addition of cost-effective carbonaceous inert materials. Yuan et al. [24] investigated the effects of steel slag and steel fibers on the shielding effectiveness of high-strength concrete (HSC). They found that steel slag had a marginal impact on the shielding effectiveness, but steel fibers significantly improved the shielding effectiveness and mechanical properties of HSC.

A few studies [9,10,25–28] have focused on the advanced technology of adding an EMI shielding function to (ultra-)high-performance cementitious composites that exhibit high strength and ductility. Jung et al. [10] added various amounts of CNTs ranging from 0 to 2 wt.% to ultra-high-performance concrete (UHPC). The results indicated improved mechanical properties owing to pore filling and bridging effects and a denser calcium silicate hydrate (C–S–H) structure for amounts below the critical incorporation concentration of 0.8–1.0 wt.%. The EMI shielding effectiveness of UHPC could be improved by increasing the CNT content up to 0.9 wt.%, which is the percolation threshold. Mazzoli et al. [28] developed EMI-resistant engineered cementitious composites by adding graphene oxide and steel fibers. The mechanical properties and shielding effectiveness of the composites were improved by adding steel fibers and graphene oxide, and the shielding effectiveness values remained stable at between 40 and 50 dB over time. Yoo et al. [25] improved the EMI shielding effectiveness of ultra-high-performance fiber-reinforced concrete by using chemically treated carbon fibers. The conductivity and shielding effectiveness were improved with the carbon fiber content, and slightly better conductivity was obtained by using chemically treated fibers. Surface treatment with nitric acid solution was the most effective for improving the shielding effectiveness, and the best performance of 49 dB at 1 GHz was achieved with a carbon fiber content of 0.1 wt.%. Park et al. [27] reported that the carbon fiber content was the dominant factor affecting the EMI shielding effectiveness of high-performance fiber-reinforced cementitious composites (HPFRCCs); moreover, the shielding mechanism was likely to be reflection rather than absorption.

High-performance cementitious materials such as UHPC and HPFRCC are also susceptible to microcrack formation due to early age shrinkage during manufacturing because of their high amounts of binding ingredients and thin sectional areas [29]. Extreme environmental conditions and unexpected external loads can also cause microcracks. However, most previous studies [10,21–28] have been conducted without considering the potential (micro)crack formation. Therefore, the influence of cracks on the EMI shielding effectiveness needs to be evaluated for practical applications. Therefore, this study aims to investigate the effect of through-crack width on the shielding effectiveness of HPFRCCs with and without carbon fibers. Four different residual crack widths ranging from 0.02 to 0.2 mm were applied through pre-loading direct tensile tests, and the pre-cracked HPFRCC samples were tested in an experimental chamber containing transmitting and receiving antennas to measure the EMI shielding effectiveness. As basic material properties, the electrical resistivity and mechanical properties of the HPFRCCs were also evaluated.

2. Test program

2.1. *Properties of ingredients and mixing process*

Type I ordinary Portland cement (OPC; Sungshin Cement Corp.), silica fume (Elkem), and fly ash (Maxcon) were used as the binding ingredients. The specific surface areas of the OPC, silica fume, and fly ash were 3700, 200,000, and 3850 cm^2/g, respectively. The chemical compositions of the binding ingredients are listed in Table 1. Silica flour with a median particle size of 14.1 μm containing 98% SiO_2 was used as filler, and quartz sand with particle sizes ranging from 100 to 800 μm was employed as fine aggregate. As reinforcements, steel fibers with a diameter of 0.2 mm and length of 19.5 mm and unsized carbon fibers with a diameter of 10 μm and length of 12 mm were incorporated. 19.5 mm steel fibers were found to be most effective for improving flexural behavior without a deterioration of fiber dispersion [30] which is very important in forming electrical network attributed to the electrical conductivity. Unsized 12 mm carbon fiber also provided the best EMI shielding effectiveness and electrical conductivity [31]. The detailed geometric and mechanical properties of the steel and carbon fibers are listed in Table 2. Because the use of fine ingredients, steel fiber, and carbon fiber reduces the fluidity of

Table 1 – Chemical compositions of the binding ingredients.

Composition %	Cement*	Silica fume	Fly ash
CaO	60.7	0.21	22.78
Al_2O_3	5.0	0.1	14.54
SiO_2	20.6	95.31	38.07
Fe_2O_3	3.4	0.35	5.42
MgO	2.6	0.8	2.67
SO_3	2.38	0.55	5.45
Na_2O	0.15	0.19	0.92
K_2O	0.98	–	5.83

the mixture, a polycarboxylate superplasticizer (SP) was adopted as a high-range water-reducing admixture to achieve proper flow values.

Two types of HPFRCC were fabricated in this study, and the detailed mixture proportions are listed in Table 3. Both HPFRCC mixtures were the same except for the carbon fiber content: 0.3 wt.% carbon-fiber based on the binding ingredients was incorporated in the HPFRCC specimen denoted HP-CF. A water-binder ratio of 0.3 was adopted, and silica fume and fly ash were added at 10% and 20% of the cement weight, respectively. Steel fibers were incorporated at 2% of the mixture volume. All of the dry ingredients (i.e., cement, silica fume, fly ash, sand, and silica flour) were blended in a Hobart-type mixer for 10 min. Once the dry ingredients and carbon fibers were well-dispersed, the water-containing SP was added and mixed for another 10 min. When the mixture exhibited proper fluidity, the steel fibers were carefully incorporated and mixed for an additional 5 min. Then, the flow value of the mixture was measured according to ASTM C1437 [32], and both the HP and HP-CF mixtures reached suitable values of 230–250 mm. A flowable fresh mixture of HPFRCC was cast in specimen molds, and the cast surfaces were covered with a plastic sheet to inhibit rapid water evaporation.

2.2. *Pre-cracking tensile tests*

For the EMI shielding tests of HPFRCCs containing a single crack, unique dog-bone-shaped specimens were fabricated, as shown in Fig. 1a. The height and width of the dog-bone-shaped specimens were 200 mm and 25 mm, respectively, to obtain plate-shaped specimens with dimensions of 200 × 200 × 25 mm^3 for the EMI shielding tests after the pre-cracking tests. To induce a single crack, a notch with a width of 5 mm and depth of 7.5 mm was generated in the middle of the specimens. Because the tensile behavior of fiber-reinforced cementitious composites is significantly affected by the fiber orientation [33], the fresh HPFRCCs were carefully arranged parallel to the direction of the tensile load for consistent results. The cast HPFRCC specimens were initially cured at room temperature for 48 h, after which the molds were removed. The demolded specimens were then cured in a steam chamber at a temperature of 90 °C for 72 h to promote strength development.

The direct tensile tests for pre-cracking were conducted using a universal testing machine (UTM) that has a load-carrying capacity of 300 kN, as shown in Fig. 1b. A uniaxial force was applied to the specimens at a rate of 0.5 mm/min, and it was measured using a load cell included in the top support. The crack-mouth opening displacement (CMOD) was measured at the center of both specimen sides using two clip-on displacement gauges (UB-5A, Tokyo Measuring Instruments Lab.). Four different single-crack widths ranging from 0.02 mm to 0.2 mm were induced by the residual CMOD after the tensile load was removed, and all induced single cracks were confirmed to be located in the notched area and to widen as the residual CMOD increased (i.e., no multiple cracks in notched area). Based on the calculation of the crack width variation by Victor C. Li [34], in which the crack width of engineered cementitious composites (ECC), a superior type of HPFRCC, expected to be ranging from 16 to 95 μm, the minimum crack width in this study was determined to be 0.02 mm (i.e., 20 μm). At least three specimens were tested and analyzed for each crack width in both the HP and HP-CF types of HPFRCC. The pre-cracked specimens were cut using a diamond saw in the middle to obtain plate-shaped specimens with dimensions of 200 × 200 × 25 mm^3 and stored in the laboratory until use in the EMI shielding tests.

2.3. *EMI shielding tests*

The EMI shielding effectiveness (SE) of the HPFRCC specimens was measured in the frequency range of 900 MHz to 2.0 GHz according to military standard MIL-STD-188-125-1 [35]. As shown in Fig. 2, an experimental chamber enclosed by metallic walls (i.e., shielding barriers) was prepared. An aperture with dimensions of 240 × 240 mm^3, into which the HPFRCC specimens were installed, was located on the testing sidewall. Two log-periodic antennas (HL033, Rohde-Schwarz) with a frequency range of 80 MHz–2000 MHz were employed as the transmitting and receiving antennas. The transmitting antenna installed outside the experimental chamber was connected to a signal generator (SMBV100A, Rohde-Schwarz) through a fiber-optic link, and the receiving antenna installed in the experimental chamber was connected to a signal analyzer (FSV, Rohde-Schwarz). The antennas were aligned with the center of the aperture, and the distance

Table 2 – Geometrical and physical properties of steel fiber and carbon fiber.

Fiber type	Diameter, d_f	Length, l_f [mm]	Aspect ratio (l_f/d_f)	Density [g/cm^3]	Tensile strength, f_f [MPa]	Elastic modulus, E_f [GPa]
Steel fiber	0.2 mm	19.5	97.5	7.9	2580	200
Carbon fiber	10 μm	12.0	1200	1.76	4900	230

Table 3 – Mixture proportions for HPFRCC specimens.

Type	W/B	Unit weight (kg/m^3)								
		Water	Cement	Silica fume	Fly ash	Sand	Silica flour	SP[a]	Steel fiber	Carbon fiber
HP	0.3	262.8	694	69.4	138.8	832.8	138.8	11.12	156	–
HP-CF	0.3	262.8	694	69.4	138.8	832.8	138.8	11.12	156	2.71

[a] Superplasticizer contains 70% water (=36.8 kg/m^3).

between the antennas was 3 m (i.e., the distances from the transmitting and receiving antennas to the wall were 2 and 1 m, respectively). The signal was generated and transmitted at 120 test frequencies ranging from 900 MHz to 2.0 GHz, and a PC was used for data acquisition and instrument control. The interior wall and floor of the experimental chamber were covered with carbon-based absorbers to minimize the reflection of the transmitted signal, which can result in an underestimated SE value.

The EMI SE of the HPFRCC specimen, expressed in decibels (dB), is defined as follows [35]:

$$SE = 20 \log \frac{V_c}{V_m}, \quad (1)$$

where V_c is the calibration signal measured without any specimen in the experimental setup, and V_m is the signal measured with the HPFRCC specimen.

The notched specimens were installed and aligned with the center of the aperture using a steel frame and tightly affixed to the wall using a clamp. To prevent signal leakage, the interfacial gaps between the wall and steel frame and between the steel frame and specimen were filled with metallic gaskets. The sides of the steel frame and specimen were also blocked using copper sticky tape.

2.4. AC impedance measurements

Prismatic specimens with dimensions of 60 × 60,× 160 mm^3 were fabricated to investigate the influence of carbon fibers on the electrical conductivity of the HPFRCC. Two copper plates with dimensions of 20 × 60 × 0.5 mm were embedded in the specimens at intervals of 30 mm as electrodes. The AC impedance of the HPFRCC specimens was measured using an LCR meter (E4980A, Keysight Technologies) in the frequency range of 1 Hz to 1 MHz.

2.5. Concept of electromagnetic shielding mechanism of HPFRCC

Shielding barriers containing conductive or magnetic materials attenuate electromagnetic waves by reflecting or absorbing energy. The electromagnetic (EM) wave incident on the shielding barrier is diminished by four different mechanisms: reflection, absorption, and multiple reflections within the shielding material [36]. As shown in Fig. 3, as the EM wave encounters the surface of the shielding barrier, part of the incident wave is reflected, referred to as reflection loss. The remaining wave penetrates the surface, and a portion of the wave is attenuated as it proceeds through the shielding

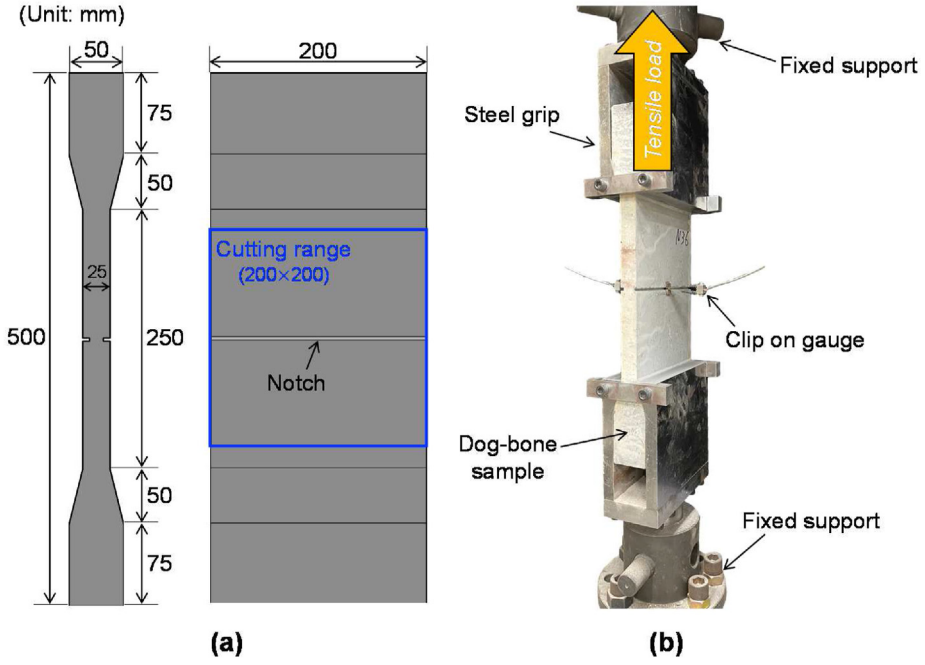

Fig. 1 – Direct tensile test setup of notched dog-bone specimen: (a) details of specimen geometry and (b) test picture.

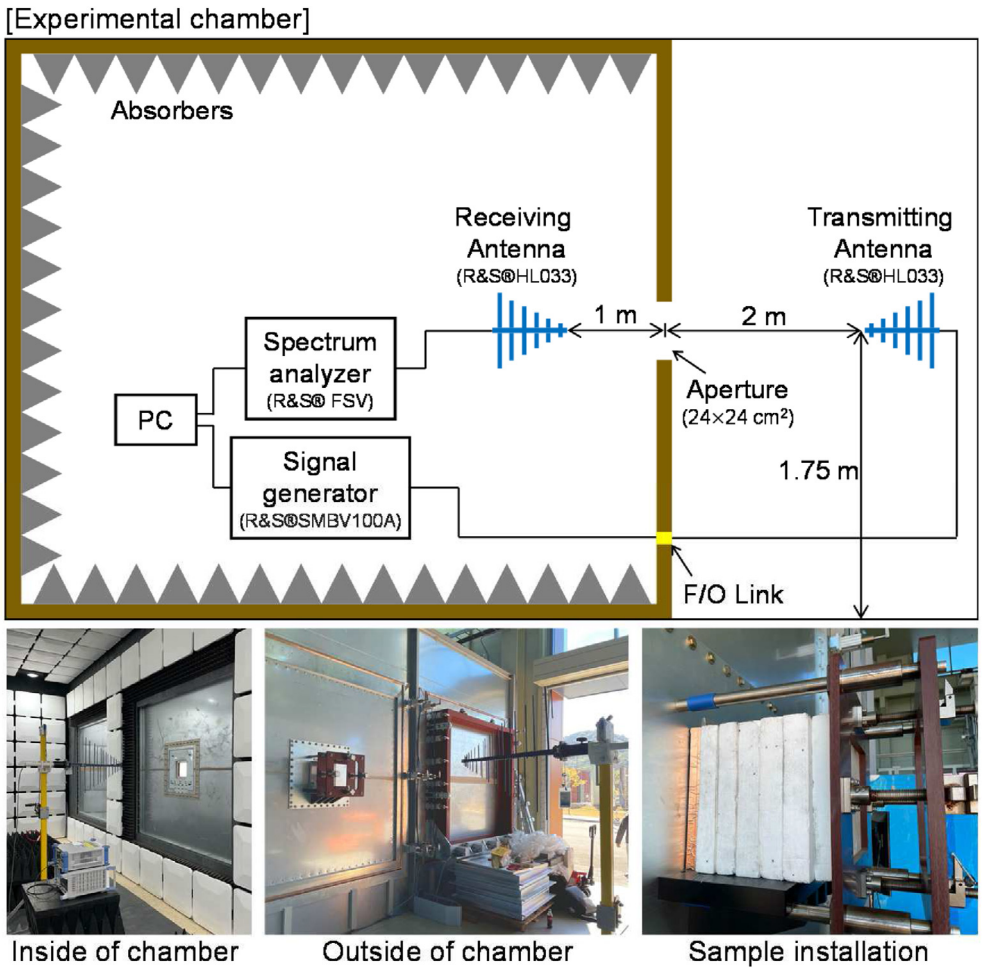

Fig. 2 – Detailed test setup for measurement of EMI shielding effectiveness.

barrier, referred to as absorption loss. When the wave strikes the inner surface of the shielding barrier, it becomes the incident wave for the interior surface; thus, part of the wave is reflected within the barrier, while the remaining wave is transmitted to the outside. The reflected wave travels through the shielding barrier again and undergoes the same process repeatedly until the energy is dissipated.

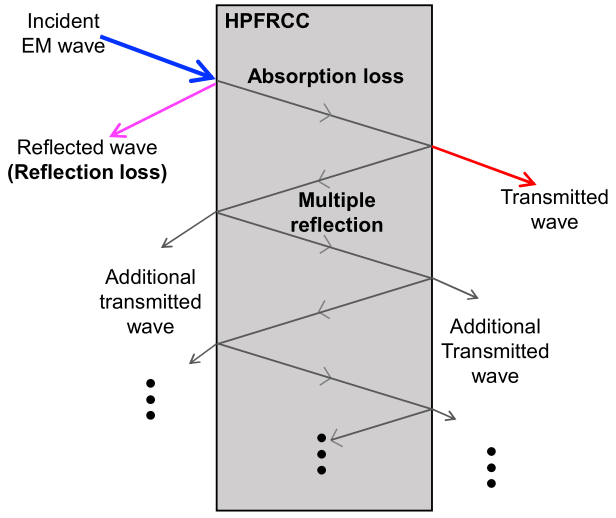

Fig. 3 – Schematic description of EMI shielding mechanisms.

The SE, defined as the ratio of the incident wave strength to the transmitted wave strength in decibels, can be divided into three terms representing the reflection loss (R_{dB}), absorption loss (A_{dB}), and loss associated with multiple reflections and transmissions (M_{dB}), as follows [36]:

$$SE_{dB} = 20\log\left|\frac{\widehat{E}_i}{\widehat{E}_t}\right| = 20\log\left|\frac{\widehat{H}_i}{\widehat{H}_t}\right| = R_{dB} + A_{dB} + M_{dB}, \quad (2)$$

where $\widehat{E}_i$ and $\widehat{H}_i$ are the magnitudes of the incident electric and magnetic fields, respectively, and $\widehat{E}_t$ and $\widehat{H}_t$ are the magnitudes of the transmitted electric and magnetic fields, respectively.

The reflection loss, R_{dB}, is attributed to the relative mismatch of the surface impedance between the incident wave and the shielding barrier [37]. The absorption loss, A_{dB}, is associated with the ohmic loss attributed to the heating of the material and the induced current in the medium [37]. The loss associated with multiple reflections and transmissions, M_{dB}, can be disregarded if the shielding materials are good conductors and their thicknesses are greater than the skin depth

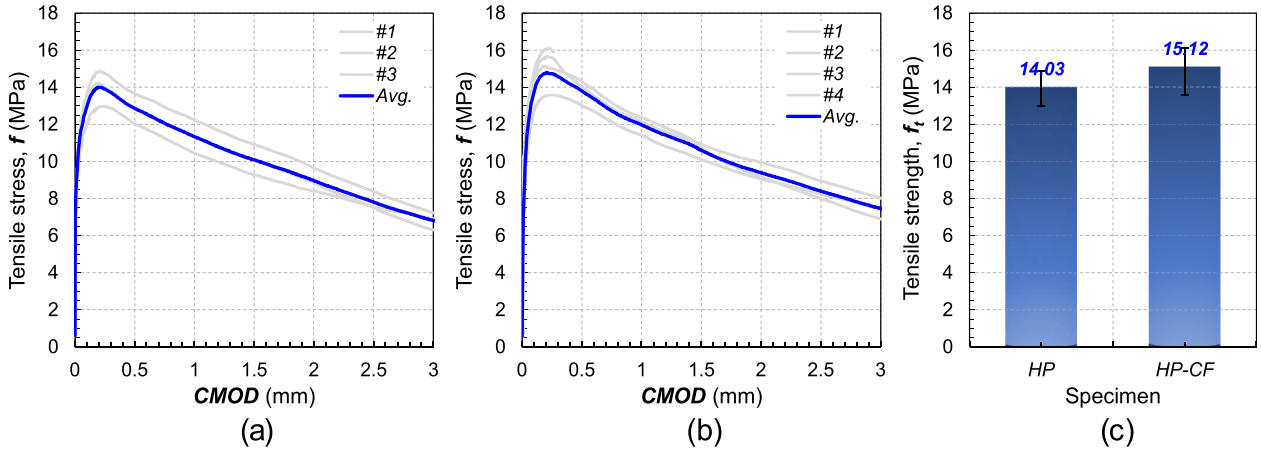

Fig. 4 – Tensile stress and strain curves of (a) HP and (b) HP-CF and (c) comparison of tensile strength.

(δ) [36]. R_{dB}, A_{dB}, and M_{dB} can be expressed by the following generalized equations [37]:

$$R_{dB} = 10\log\left(\frac{\sigma_T}{16f\varepsilon\mu_r}\right), \quad (3)$$

$$A_{dB} = 8.68t\frac{\sqrt{(f\mu_r\sigma_T)}}{2}, \quad (4)$$

$$M_{dB} = 20\log\left(e^{-\frac{2t}{\delta}}\right), \quad (5)$$

where σ_T is the electrical conductivity, ε is the dielectric permittivity, μ_r is the relative magnetic permeability, t is the thickness of the shielding material, and f is the frequency of the incident wave.

As shown in the above equations, the SE depends on the frequency, electrical conductivity, and relative magnetic permeability. Cementitious composites, including HPFRCCs, contain high amounts of water compared to other composites. Water has a very high dielectric permittivity; therefore, the moisture content in cementitious composites is a crucial factor for achieving better EM SE [38,39]. In addition, the absorption of EM waves can be improved by increasing the porosity of cementitious composites, as this allows for a greater number of multiple reflections at the interface between the air and matrix [40]. Steel fibers incorporated in HPFRCCs exhibit high electric permittivity and relative permeability and provide higher EM SE owing to the dielectric loss and magnetic hysteresis loss [41].

3. Test results and discussion

3.1. Tensile behavior

Fig. 4 shows the tensile stress and CMOD curves of the HPFRCCs with and without carbon fibers. Owing to the excellent crack-bridging capability of 2 vol.% straight steel fibers, all of the tested HPFRCCs exhibited a higher load-carrying capacity even after the formation of the initial penetration crack. An average tensile strength of 14.03 MPa was found in the plain HPFRCC (HP sample), and it increased by 7.8% with the addition of 0.2 vol.% carbon fibers (HP-CF sample). This is due to the excellent interfacial bond strength of steel fibers in UHPC (5.95 MPa), given they are aligned [42]. The CMOD value corresponding to the maximum tensile strength was approximately 0.21 mm for both the HP and HP-CF samples. Carbon fibers are hydrophobic, thus leading to poor dispersibility and low interfacial bonding with the cement matrix [25]. However, owing to their very small cross-sectional diameter ($\leq$0.01 mm), sufficient carbon fibers bridged the crack, even though the volume fraction was only 0.2%. Therefore, the tensile strength of the HPFRCC increased to 15.12 MPa. In Fig. 5, the carbon fibers bridged the cracks along with the steel

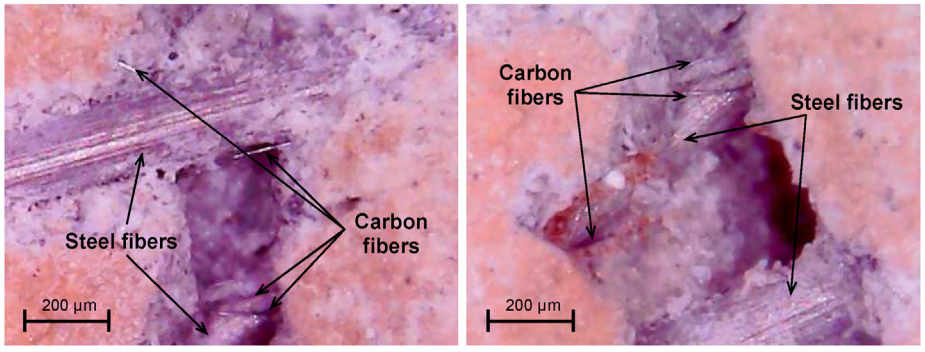

Fig. 5 – Picture of localized crack surface.

fibers, which enhanced the tensile performance of the HPFRCC. In addition, it was verified that the carbon fibers were significantly smaller than the steel fibers. Thus, a greater number of carbon fibers than steel fibers were detected at the crack surface, although the volume fraction of carbon fibers (0.2%) was a tenth of the volume fraction of steel fibers.

To evaluate the influence of the penetrating crack width on the EMI SE of the HPFRCCs, four different residual pre-crack widths were considered: 0.02, 0.04, 0.1, and 0.2 mm. Pre-tensile tests were conducted to generate the cracks, and the tensile stress and CMOD curves are shown in Fig. 6. Because steel and carbon fibers are randomly oriented and dispersed in

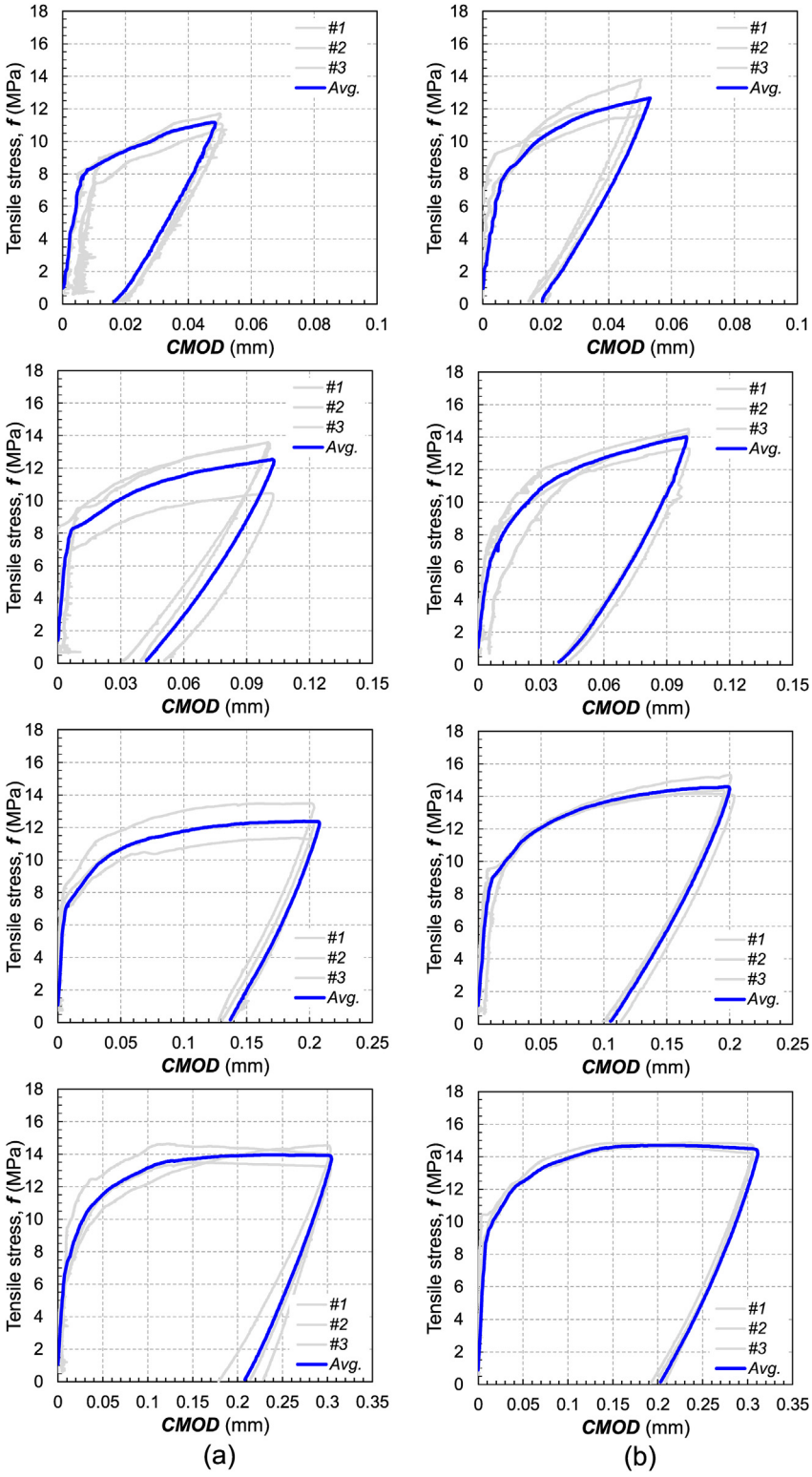

Fig. 6 – Summary of pre-cracking tensile behaviors: (a) HP and (b) HP-CF.

the composites [33,43], high data deviations are obtained. This is because the pullout behavior of the fibers from the cement matrix varies according to the inclination angle, which is attributed to the snubbing friction and matrix spalling effects [44]. Lee et al. [45] experimentally verified the changes in the bond strength and pullout work of steel fibers from UHPC based on their inclination angle. Based on micromechanical analysis. Yoo et al. [46] reported that the bridging capacity of multiple fibers at a crack surface was affected by the orientation of the fibers. A two-dimensional random orientation leads to a higher fiber bridging strength than a three-dimensional random orientation. Therefore, owing to the high data variability, it was difficult to achieve consistent residual crack widths. The pre-cracking tensile tests were designed to be unloaded at target crack widths of 0.05, 0.1, 0.2, and 0.3 mm. In this process, the residual crack widths were effectively controlled to 0.02, 0.04, 0.1, and 0.2 mm, respectively. The maximum tensile strengths were obtained for CMOD values of 0.2 mm and 0.3 mm. The HPFRCC samples with residual crack widths of 0.2 mm were thus included in the softening region with crack localization. On the other hand, the samples with residual crack widths of 0.1 mm or smaller (0.02 and 0.04 mm) were located in the ascending region before the crack localization. Theoretically, this means that the steel fibers at the crack surface were partially debonded and did not slip when the residual crack width was 0.1 mm or less. Fig. 7 verifies that the residual crack widths measured by the clip gauges were precise based on the enlarged images. For example, the HPFRCC samples with a residual CMOD of 0.02 mm exhibited crack widths of approximately 20.6–21.3 μm.

3.2. *Electrical conductivity*

To evaluate the influence of carbon fibers on the electrical resistance of HPFRCC, the Nyquist plots based on electrochemical impedance spectroscopy are compared in Fig. 8(a), where the y-axis is the imaginary impedance, Im(z), and the x-axis is the real impedance, Re(z). Two samples were prepared for each variable, and the average bulk resistance value was used to compare the electrical properties. The Nyquist plot consists of a bulk arc and electrode arc [47]. Wansom et al. [48] and Park et al. [27] reported two bulk arcs based on a cement matrix and conductive materials such as multi-wall CNTs and carbon fibers. However, this study and other researchers [26,49] also noted that the low-frequency bulk arc, which is based on the contribution of the cement matrix, overlaps with the electrode arc, leading to a single bulk arc. As shown in Fig. 8, the electrical resistance of the HPFRCC was significantly decreased with the addition of 0.2 vol.% carbon fibers. For instance, the average bulk resistance of the HP specimen was 22,395 Ω, whereas that of the HP-CF specimen was 6510 Ω. Based on the average bulk resistance, the electrical resistivity (ρ) and conductivity (σ) of HP and HP-CF specimen were calculated using following equations:

$$\rho_b = \frac{R_b A}{l}, \tag{6}$$

$$\sigma_b = \frac{1}{\rho_b}, \tag{7}$$

where R_b is the averaged electrical resistance, A is the contact cross-sectional area between the electrode and specimen, and l is the distance between the electrodes. The calculated electrical resistivity and conductivity of HP and HP-CF specimens are shown in Fig. 8(b). The electrical conductivity of HP-CF specimen was 3.84×10^{-3} S/m which was approximately 224% higher than that of HP specimen. This is because the addition of carbon fibers helps form electrical pathways more effectively. Even though the electrical conductivity is relatively low in comparison with that of steel fibers, the higher aspect ratio of carbon fibers is effective for connecting the conductivity network [50]. The benefits for improving the electrical conductivity of steel fiber-reinforced cement composites with the addition of carbon fibers were comprehensively reported by Yoo et al. [9] and Nguyen et al. [51]. In particular, as shown in Fig. 5, not only can the carbon fibers connect with each other, but they can also connect to the steel

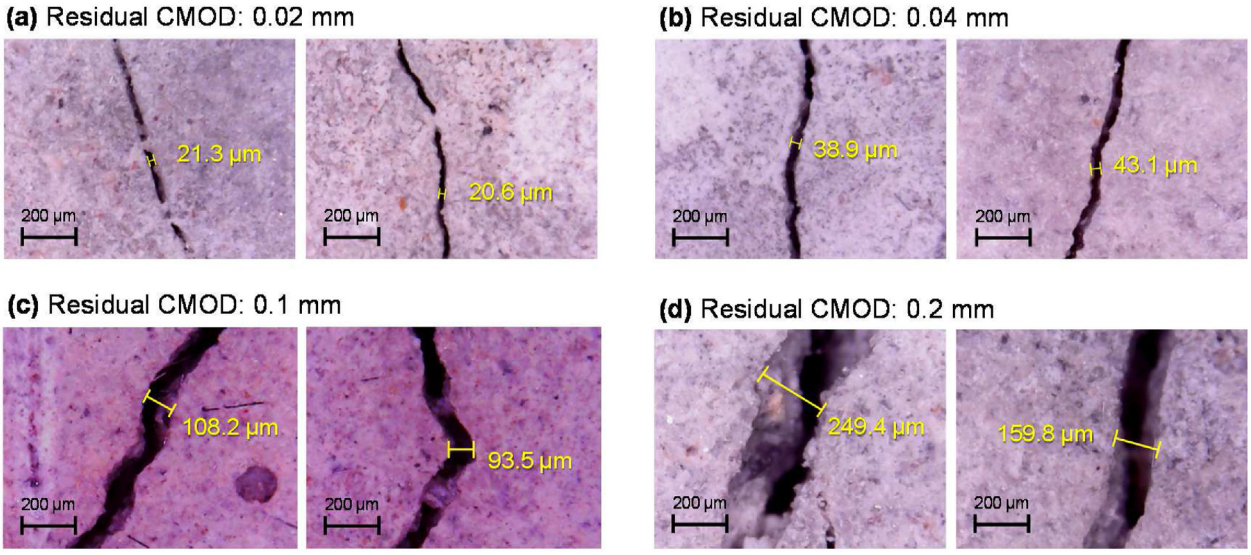

Fig. 7 – Pictures of various crack widths: (a) 0.02 mm, (b) 0.04 mm, (c) 0.1 mm, and (d) 0.2 mm.

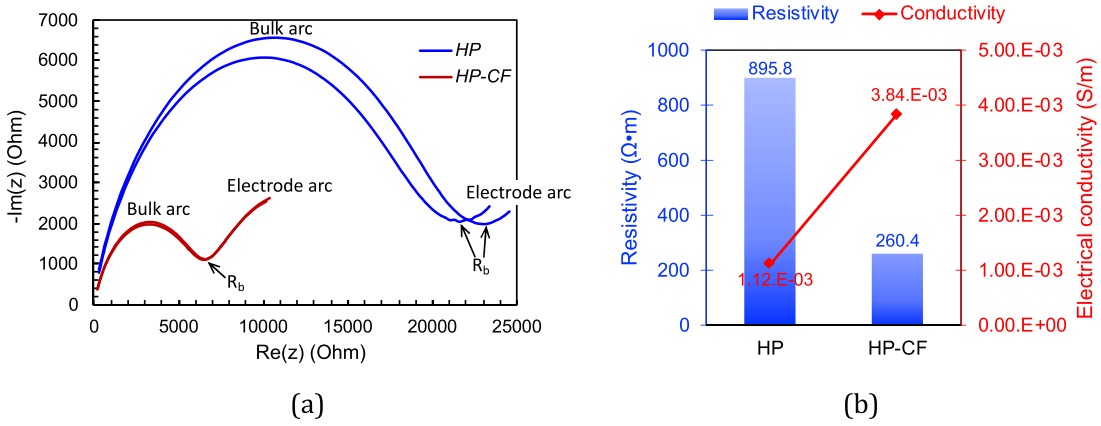

Fig. 8 – Electrical properties of HP and HP-CF: (a) Nyquist plots and (b) Electrical resistivity and conductivity.

fibers, which helps form electron pathways that reduce the electrical resistance.

3.3. *EMI shielding effectiveness*

3.3.1. *Effect of carbon fibers*

Fig. 9 summarizes the EMI SE versus frequency curves for the non-cracked HP and HP-CF samples. To obtain reliable test results, three samples were analyzed for each variable, and an average curve was used for comparison. The SE was measured in both the horizontal and vertical directions of the log-periodic antennas. The SE measured by the antenna horizontal to the direction of the notch was slightly lower than that measured by the vertical antenna because the notches formed to generate a single crack in the HPFRCC samples. Owing to the notch (width of 5 mm and depth of 7.5 mm), the cross-sectional depth at the center decreased from 25 to 10 mm. This is consistent with the findings of previous studies [9,52]. Shukla [52] reported that the absorptive capacity of EM waves was proportional to the conductivity, permeability, and thickness of the medium. Yoo et al. [9] also found that a significant decrease in the HPFRCC panel thickness resulted in deterioration of its EMI SE. For conservative data analysis, the SE measured by the vertical antenna was used in this study to obtain the average curve shown in Fig. 10.

The addition of a small amount of carbon fibers (0.3 wt.% of the cementitious materials) effectively improved the SE of the HPFRCC, as shown in Fig. 10. This is consistent with the findings of Yoo et al. [9], who reported that both the electrical conductivity and SE were improved by adding carbon fibers. Ozturk and Chung [53] also reported the benefits of carbon fibers for enhancing the conductivity and SE of cement pastes. A higher carbon fiber content led to a better enhancement of the conductivity and SE. This was attributed to the formation of more electrical pathways and improved connectivity. The conductive network formed by the carbon fibers caused an oscillating current that converted EM energy to thermal energy [38]. An increase in the conductivity of cement paste with

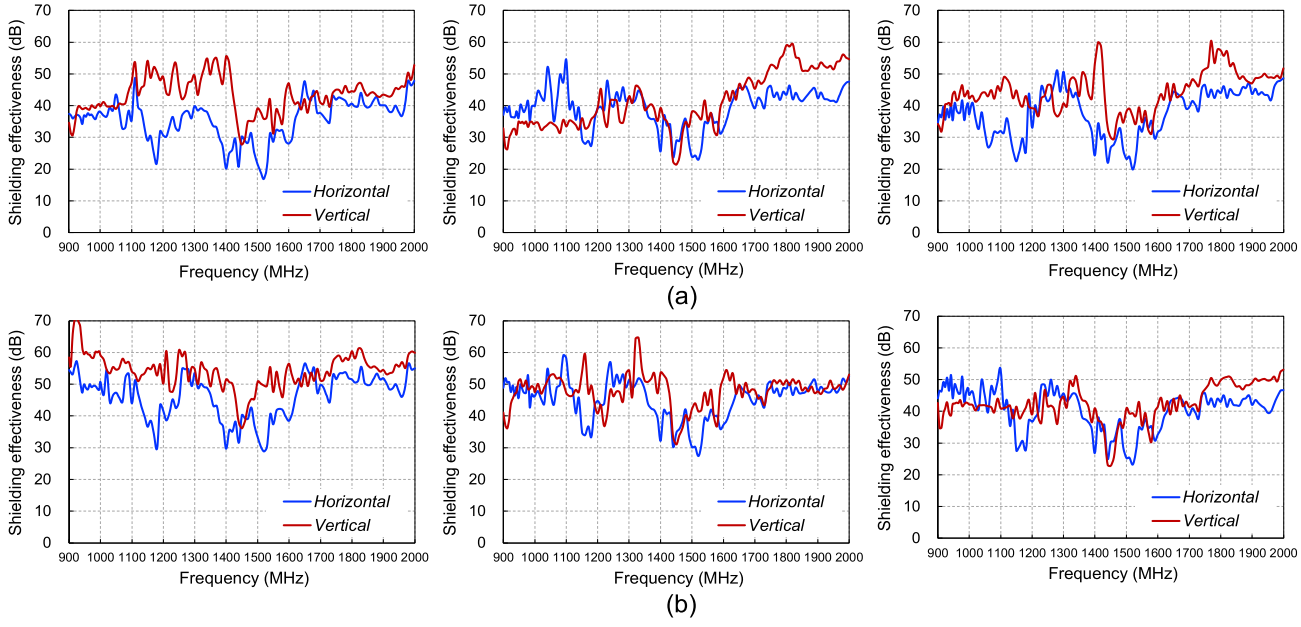

Fig. 9 – Summary of EMI shielding effectiveness of non-cracked HPFRCCs: (a) HP and (b) HP-CF.

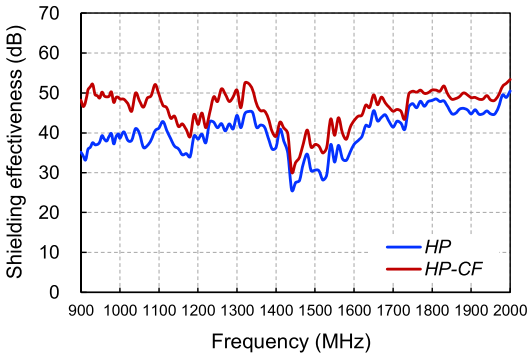

Fig. 10 – Effect of carbon fibers on the shielding effectiveness of HPFRCC.

the addition of carbon fibers was also reported by Wen and Chung [54]. In addition, because the dispersion of conductive particles such as carbon and steel fibers produces internal reflection of incident waves within the medium [55], the additional carbon fibers in the HP-CF samples provided greater scattering of EM waves in the matrix, resulting in higher SE than that of the HP samples containing only steel fibers. At a frequency of 1 GHz, the SE of the HP-CF specimen averaged 48.5 dB, which was approximately 26% higher than that of the HP specimen. This is an excellent SE because a thin plate specimen with a dominant thickness of 10 mm was used for the EMI shielding tests. In addition, from 900 MHz to 2 GHz, the HP-CF specimens provided higher SE than the corresponding HP specimens, regardless of the frequency.

3.3.2. *Effects of the crack and its width*

Figs. 11 and 12 show the average SE versus frequency curves for the HP and HP-CF samples with varying crack widths and directions of the antenna. It is evident that the SE measured by the antenna horizontal to the cracks was significantly lower than that measured by the vertical antenna for all cracked samples. This is caused by the transmission of EM waves through the penetrated cracks. The discrepancies between the SE values with different antenna directions were not significantly influenced by the crack width or the presence of carbon fibers in the HPFRCC. In a previous study [9], the SE of HPFRCC panels was not decreased by a single microcrack, but decreased with multiple microcracks and crack localization. The singly cracked HPFRCC panels maintain sufficient EMI SE owing to the non-cracked compressive section under flexure [9]. However, the SE of the HPFRCC specimens was significantly reduced by the formation of even tiny single cracks with a width of 20 μm because the crack penetrated the entire cross-section of the dog bone specimens. At the through-crack surface, EM waves can easily penetrate the spaces between the bridging fibers. Moreover, the decrement of the electrical conductivity caused by crack also affects the degradation of the SE. Generally, the crack opening incurs the reduction of the electrical conductivity of HPFRCC because the conductive path attributed to the connection between the steel fibers are

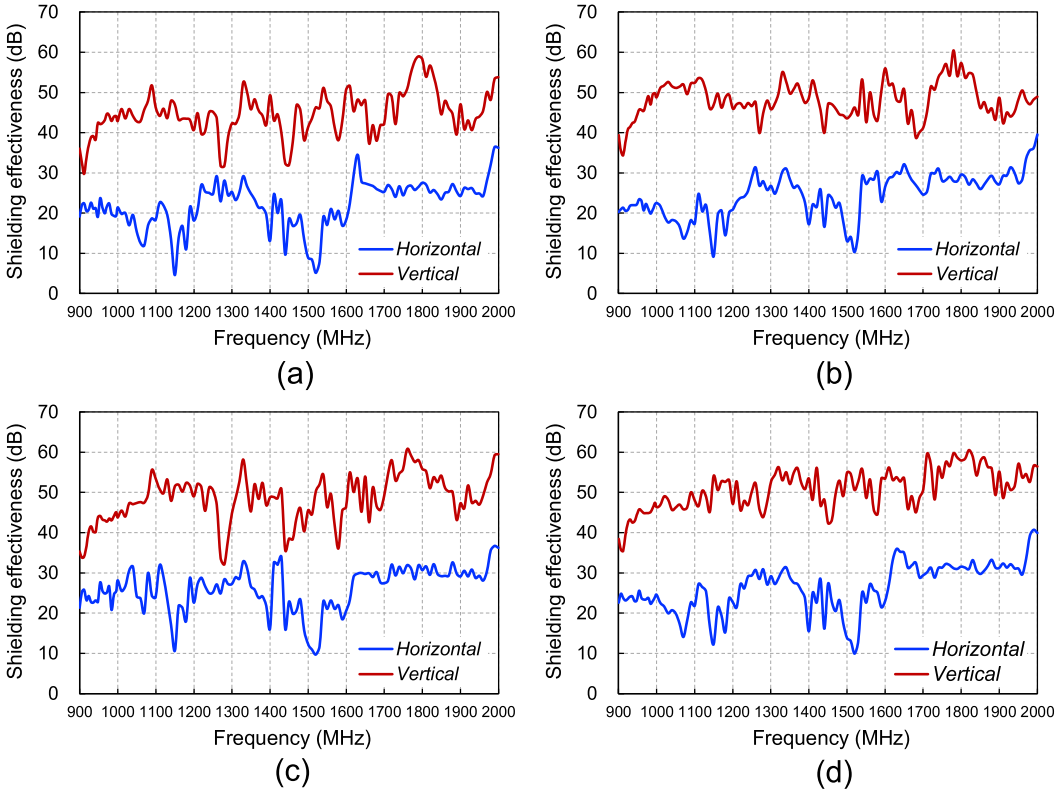

Fig. 11 – Comparison of shielding effectiveness of cracked HP specimen according to antenna direction with residual crack widths of (a) 0.02 mm, (b) 0.04 mm, (c) 0.1 mm, and (d) 0.2 mm.

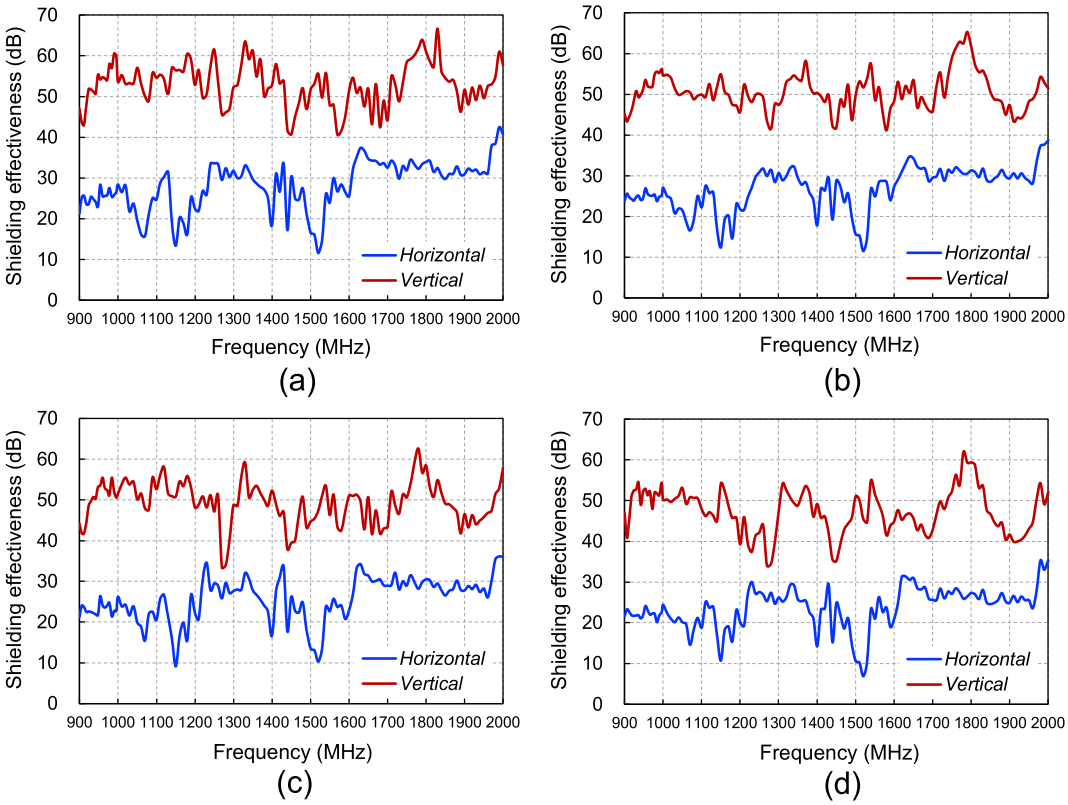

Fig. 12 – Comparison of shielding effectiveness of cracked HP-CF specimen according to antenna direction with residual crack widths of (a) 0.02 mm, (b) 0.04 mm, (c) 0.1 mm, and (d) 0.2 mm.

lost. Huy Viet Le and Dong Joo Kim [56], found out the electrical resistivity started to increase after the debonding between matrix and steel fibers occurs, and the fiber slip after the debonding resulted in the higher electrical resistivity, which indicates the crack bridged by the fibers widens. For instance, the HP specimen with a 0.02 mm pre-crack showed an SE of 21.4 dB at 1 GHz, approximately 44% lower than the specimen without a crack.

The effect of the crack width on the SE of the HP and HP-CF specimens is shown in Fig. 13. Apparently, the SE of both HP and HP-CF samples significantly decreased owing to through-crack formation. However, the SE of the cracked HPFRCC was not significantly affected by the crack width. This means that the SE versus frequency curves of HP were quite similar for crack widths of 0.02 mm–0.2 mm. For instance, for crack widths from 0.02 to 0.2 mm, the EMI SE values for HP specimens were approximately 21.4–28.2 dB at a frequency of 1 GHz (Fig. 14), which were approximately 27%–44% lower than the SE values for non-cracked HP samples. This insignificant effect of crack width on EMI SE can be attributed to the dispersion of the steel fibers. Considering the EMI shielding mechanism after crack occurs, the size of crack is neglectable as compared to the size of steel fibers considering. Because a portion of matrix on the EMI shielding is dissipated once a crack occurs, only the connection between steel fibers contributes to the EMI SE. However, the SE of the HP-CF samples

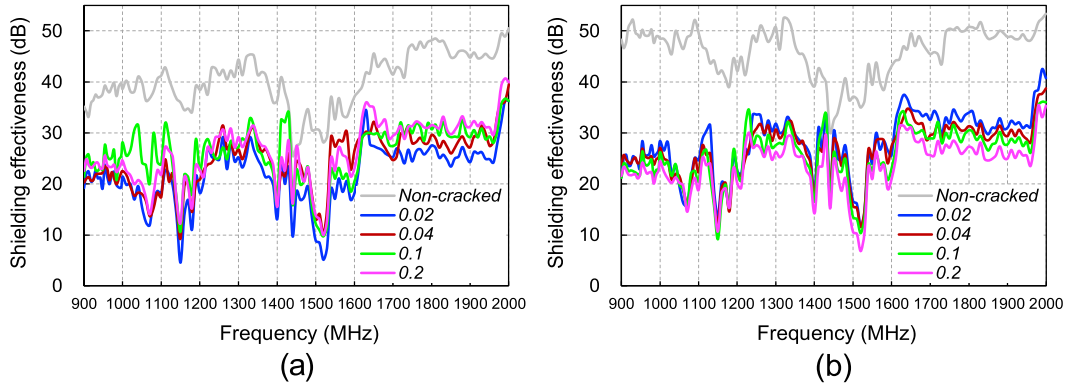

Fig. 13 – Effect of residual crack width on EMI shielding effectiveness of HPFRCC: (a) HP and (b) HP-CF [unit: mm].

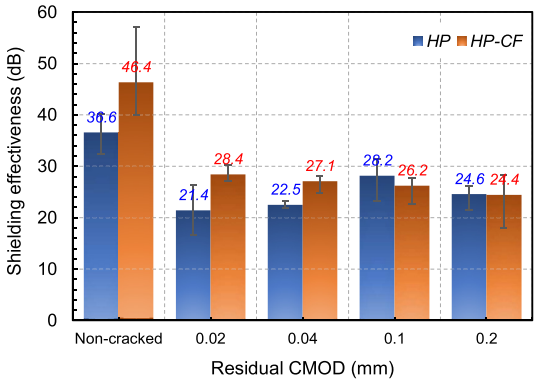

Fig. 14 – Comparative shielding effectiveness at 1 GHz.

gradually decreased with increasing crack width. At tiny crack surfaces (up to a width of 0.04 mm), the carbon fibers helped shield the EM wave transmission owing to the high fiber numbers. Although the volume of carbon fibers was considerably lower (0.2%), the number of carbon fibers was sufficiently high because of the smaller cross-sectional area and high aspect ratio. However, the benefits of adding 0.2 vol.% carbon fibers in enhancing the SE of HPFRCC disappeared at crack widths of 0.1 mm or greater. Therefore, the SE values of the HP and HP-CF specimens were similar at 1 GHz (24.4–24.6 dB). This indicates that the carbon fibers were effective only for non-cracked HPFRCCs or HPFRCCs with very small cracks (≤0.04 mm). Compared to the SE of the non-cracked HP-CF specimens, the cracked HP-CF specimens showed an SE that was approximately 41%–50% lower.

4. Conclusions

This study investigated the effects of the incorporation of carbon fibers and the crack width on the EMI SE of HPFRCCs. Pre-cracks were formed under tension with four different widths ranging from 0.02 to 0.2 mm. The mechanical and electrical properties were evaluated. Based on the test results and discussion above, the following conclusions can be drawn.

1) The addition of 0.2 vol.% carbon fibers effectively improved the tensile strength, electrical conductivity, and EMI SE of the HPFRCC.
2) The electrical conductivity of HP-CF was 3.84×10^{-3} S/m, which was approximately 224% higher than that of HP; the SE of HP-CF was found to be 48.5 dB at 1 GHz, which was approximately 26% higher than that of HP.
3) The SE of HPFRCCs with and without carbon fibers was significantly reduced owing to the formation of even tiny cracks with a width of 20 μm. At 1 GHz, the SE of HP and HP-CF specimens was reduced by approximately 40% with formation of a 20 μm crack.
4) The SE of the thoroughly cracked HP specimens was not significantly influenced by the crack width. However, with the addition of carbon fibers (HP-CF), the SE gradually decreased with increasing crack width because the carbon fibers helped shield the EM waves at tiny crack surfaces of up to 40 μm.
5) The added carbon fibers were effective only for HPFRCCs without cracks or with cracks of less than 40 μm. Thus, the SE of HP and HP-CF was similar at crack widths of 0.1 mm or greater.

Declaration of Competing Interest

The authors declare that they have no known competing financial interests or personal relationships that could have appeared to influence the work reported in this paper.

Acknowledgements

This research was supported by a Grant (22SCIP–C146646-05) from the Construction Technology Research Project funded by the Ministry of Land, Infrastructure, and Transport of the Korean government.

REFERENCES

[1] Chung DDL. Cement reinforced with short carbon fibers: a multifunctional material. Compos B Eng 2000;31(6–7):511–26.
[2] Lavagna L, Musso S, Ferro G, Pavese M. Cement-based composites containing functionalized carbon fibers. Cem Concr Compos 2018;88:165–71.
[3] Han B, Zhang L, Zhang C, Wang Y, Yu X, Ou J. Reinforcement effect and mechanism of carbon fibers to mechanical and electrically conductive properties of cement-based materials. Construct Build Mater 2016;125:479–89.
[4] Chen PW, Chung DDL. Low-drying-shrinkage concrete containing carbon fibers. Compos B Eng 1996;27(3–4):269–74.
[5] Wongtanakitcharoen T, Naaman AE. Unrestrained early age shrinkage of concrete with polypropylene, PVA, and carbon fibers. Mater Struct 2007;40(3):289–300.
[6] Yoo DY, You I, Zi G, Lee SJ. Effects of carbon nanomaterial type and amount on self-sensing capacity of cement paste. Measurement 2019;134:750–61.
[7] Azhari F, Banthia N. Cement-based sensors with carbon fibers and carbon nanotubes for piezoresistive sensing. Cem Concr Compos 2012;34(7):866–73.
[8] D'Alessandro A, Rallini M, Ubertini F, Materazzi AL, Kenny JM. Investigations on scalable fabrication procedures for self-sensing carbon nanotube cement-matrix composites for SHM applications. Cem Concr Compos 2016;65:200–13.
[9] Yoo DY, Kang MC, Choi HJ, Shin W, Kim S. Electromagnetic interference shielding of multi-cracked high-performance fiber-reinforced cement composites–Effects of matrix strength and carbon fiber. Construct Build Mater 2020;261:119949.
[10] Jung M, Lee YS, Hong SG, Moon J. Carbon nanotubes (CNTs) in ultra-high performance concrete (UHPC): dispersion, mechanical properties, and electromagnetic interference (EMI) shielding effectiveness (SE). Cement Concr Res 2020;131:106017.
[11] Singh AP, Gupta BK, Mishra M, Chandra A, Mathur RB, Dhawan SK. Multiwalled carbon nanotube/cement

composites with exceptional electromagnetic interference shielding properties. Carbon 2013;56:86–96.
[12] Chung DDL. Electrically conductive cement-based materials. Adv Cement Res 2004;16(4):167–76.
[13] Ozturk M, Chung DDL. Enhancing the electromagnetic interference shielding effectiveness of carbon-fiber reinforced cement paste by coating the carbon fiber with nickel. J Build Eng 2021;41:102757.
[14] Jia LC, Jia XX, Sun WJ, Zhang YP, Xu L, Yan DX, et al. Stretchable liquid metal-based conductive textile for electromagnetic interference shielding. ACS Appl Mater Interfaces 2020;12:53230–8.
[15] Huang FW, Yang QC, Jia LC, Yan DX, Li ZM. Aramid nanofiber assisted preparation of self-standing liquid metal-based films for ultrahigh electromagnetic interference shielding. Chem Eng J 2021;426:131288.
[16] Jia LC, Zhou CG, Sun WJ, Xu L, Yan DX, Li ZM. Water-based conductive ink for highly efficient electromagnetic interference shielding coating. Chem Eng J 2020;384:123368.
[17] Jia LC, Xu L, Ren F, Ren PG, Yan DX, Li ZM. Stretchable and durable conductive fabric for ultrahigh performance electromagnetic interference shielding. Carbon N Y 2019;144:101–8.
[18] Kim M, Kim S, Seong YC, Yang KH, Choi H. Multiwalled carbon nanotube buckypaper/polyacrylonitrile nanofiber composite membranes for electromagnetic interference shielding. ACS Appl Nano Mater 2021;4(1):729–38.
[19] https://www.who.int/peh-emf/about/WhatisEMF/en/index1.html.
[20] Yu L, Lan X, Wei C, Li X, Qi X, Xu T, et al. MWCNT/NiO-Fe_3O_4 hybrid nanotubes for efficient electromagnetic wave absorption. J Alloys Compd 2018;748:111–6.
[21] Fan Y, Zhang L, Volski V, Vandenbosch GA, Blanpain B, Guo M. Utilization of stainless-steel furnace dust as an admixture for synthesis of cement-based electromagnetic interference shielding composites. Sci Rep 2017;7(1):1–8.
[22] Singh AP, Mishra M, Chandra A, Dhawan SK. Graphene oxide/ferrofluid/cement composites for electromagnetic interference shielding application. Nanotechnology 2011;22(46):465701.
[23] Khushnood RA, Ahmad S, Savi P, Tulliani JM, Giorcelli M, Ferro GA. Improvement in electromagnetic interference shielding effectiveness of cement composites using carbonaceous nano/micro inerts. Construct Build Mater 2015;85:208–16.
[24] Yuan TF, Choi JS, Kim SK, Yoon YS. Assessment of steel slag and steel fiber to control electromagnetic shielding in high-strength concrete. KSCE J Civ Eng 2021;25(3):920–30.
[25] Yoo DY, Kang MC, Choi HJ, Shin W, Kim S. Influence of chemically treated carbon fibers on the electromagnetic shielding of ultra-high-performance fiber-reinforced concrete. Arch Civ Mech Eng 2020;20(4):1–15.
[26] Lee N, Kim S, Park G. The effects of multi-walled carbon nanotubes and steel fibers on the AC impedance and electromagnetic shielding effectiveness of high-performance, fiber-reinforced cementitious composites. Materials 2019;12(21):3591.
[27] Park G, Kim S, Park GK, Lee N. Influence of carbon fiber on the electromagnetic shielding effectiveness of high-performance fiber-reinforced cementitious composites. J Build Eng 2021;35:101982.
[28] Mazzoli A, Corinaldesi V, Donnini J, Di Perna C, Micheli D, Vricella A, et al. Effect of graphene oxide and metallic fibers on the electromagnetic shielding effect of engineered cementitious composites. J Build Eng 2018;18:33–9.
[29] Yoo DY, Min KH, Lee JH, Yoon YS. Shrinkage and cracking of restrained ultra-high-performance fiber-reinforced concrete slabs at early age. Construct Build Mater 2014;73:357–65.
[30] Yoo DY, Kang ST, Yoon YS. Effect of fiber length and placement method on flexural behavior, tension-softening curve, and fiber distribution characteristics of UHPFRC. Construct Build Mater 2014;64:67–81.
[31] Wanasinghe D, Aslani F, Ma G. Electromagnetic shielding properties of carbon fibre reinforced cementitious composites. Construct Build Mater 2020;260:120439.
[32] ASTM C1437-15. Standard test method for flow of hydraulic cement mortar, vols. 1–2; 2015.
[33] Kang ST, Kim JK. The relation between fiber orientation and tensile behavior in an ultra high performance fiber reinforced cementitious composites (UHPFRCC). Cement Concr Res 2011;41(10):1001–14.
[34] Li VC. Tailoring ECC for Special Attributes : Rev 2012;6:135–44.
[35] MIL-STD-188-125-1. High-Altitude electromagnetic (HEMP) protection for ground based C41. Facilities 2005;1–106.
[36] Paul CR. Introduction to electromagnetic compatibility. John Wiley & Sons; 2006. p. 713–52.
[37] Sankaran S, Deshmukh K, Ahamed MB, Khadheer Pasha SK. Recent advances in electromagnetic interference shielding properties of metal and carbon filler reinforced flexible polymer composites: a review. Composer Part A Appl Sci Manuf 2018;114:49–71.
[38] Hyun SY, Du JK, Lee HJ, Lee KW, Lee JH, Jung C, et al. Analysis of shielding effectiveness of reinforced concrete against high-altitude electromagnetic pulse. IEEE Trans Electromagn C 2014;56:1488–96.
[39] Bourdi T, Rhazi JE, Boone F, Ballivy G. Application of Jonscher model for the characterization of the dielectric permittivity of concrete. J Phys D Appl Phys 2008;41.
[40] Dai Y, Sun M, Liu C, Li Z. Electromagnetic wave absorbing characteristics of carbon black cement-based composites. Cem Concr Compos 2010;32:508–13.
[41] Ma G, Sun J, Aslani F, Huang Y, Jiao F. Review on electromagnetic wave absorbing capacity improvement of cementitious material. Construct Build Mater 2020:262.
[42] Yoo DY, Kim S, Kim JJ, Chun B. An experimental study on pullout and tensile behavior of ultra-high-performance concrete reinforced with various steel fibers. Construct Build Mater 2019;206:46–61.
[43] Van Mier JGM, Ruiz G, Andrade C, Yu RC. Fiber orientation in ultra high performance fiber reinforced concrete and its visualization. In: Proceedings of the 8th International Conference on Fracture Mechanics of Concrete and Concrete Structures, FraMCos-8, 10-14 March; 2013. Toledo, Spain.
[44] Li VC, Wang Y, Backer S. Effect of inclining angle, bundling and surface treatment on synthetic fibre pull-out from a cement matrix. Composer 1990;21(2):132–40.
[45] Lee Y, Kang ST, Kim JK. Pullout behavior of inclined steel fiber in an ultra-high strength cementitious matrix. Construct Build Mater 2010;24(10):2030–41.
[46] Yoo DY, Kang ST, Banthia N, Yoon YS. Nonlinear finite element analysis of ultra-high-performance fiber-reinforced concrete beams. Int J Damage Mech 2017;26(5):735–57.
[47] Neithalath N, Jain J. Applications of electrical impedance methods in linking structure of micro-and macro-porous concretes to their transport properties. In: ACI Spring 2010 convention; 2010. p. 33–50.
[48] Wansom S, Kidner NJ, Woo LY, Mason TO. AC-impedance response of multi-walled carbon nanotube/cement composites. Cem Concr Compos 2006;28(6):509–19.
[49] Hixson AD, Woo LY, Campo MA, Mason TO, Garboczi EJ. Intrinsic conductivity of short conductive fibers in composites by impedance spectroscopy. J Electroceram 2001;7(3):189–95.
[50] Xie S, Ji Z, Zhu L, Zhang J, Cao Y, Chen J, et al. Recent progress in electromagnetic wave absorption building materials. J Build Eng 2020;27.

[51] Nguyen DL, Kim DJ, Thai DK. Enhancing damage-sensing capacity of strain-hardening macro-steel fiber-reinforced concrete by adding low amount of discrete carbons. Materials 2019;12(6):938.
[52] Shukla V. Review of electromagnetic interference shielding materials fabricated by iron ingredients. Nanoscale Adv 2019;1(5):1640–71.
[53] Ozturk M, Chung DDL. Enhancing the electromagnetic interference shielding effectiveness of carbon-fiber reinforced cement paste by coating the carbon fiber with nickel. J Build Eng 2021;41:102757.
[54] Wen S, Chung DDL. The role of electronic and ionic conduction in the electrical conductivity of carbon fiber reinforced cement. Carbon 2006;44(11):2130–8.
[55] Khalid T, Albasha L, Qaddoumi N, Yehia S. Feasibility study of using electrically conductive concrete for electromagnetic shielding applications as a substitute for carbon-laced polyurethane absorbers in anechoic chambers. IEEE Trans Antenn Propag 2017;65:2428–35.
[56] Le HV, Kim DJ. Effect of matrix cracking on electrical resistivity of high performance fiber reinforced cementitious composites in tension. Construct Build Mater 2017;156:750–60.